Experimental and numerical investigations on the energy performance of a thermo-active tunnel

Experimental and numerical investigations on the energy performance of a thermo-active tunnel

A. Insana, M. Barla

Department of Structural, Building and Geotechnical Engineering, Politecnico di Torino, Torino, Italy
marco.barla@polito.it

Abstract

The paper illustrates the experimental and numerical study performed to assess the energy performance of a thermo-active tunnel lining. The experimental data from the real-scale energy tunnel prototype tested in the tunnel of the Turin Metro Line 1 South Extension are considered, by presenting the results of the tests performed in heating and cooling mode through both the ground and air configurations of the novel Enertun layout. Thanks to the availability of the original experimental data collected, it was possible to calibrate and corroborate a thermo-hydraulic numerical model, then used to extend the results to different ground and environmental conditions. Understanding of the role of some of the most important design parameters is illustrated in the form of parametric design charts, that update to the Enertun configuration those already existing in literature. A simple method for preliminary evaluation of the potential of energy tunnels, accounting for the investigated design parameters, is formulated.

Keywords: energy tunnel; thermal performance; geothermal energy; tunnel lining; design charts.

Highlights

- Thermal performance of a real scale prototype of energy tunnel system is evaluated.
- The role of groundwater flow direction and of other design aspects is studied.
- Updated preliminary thermal design charts are built and validated.
- A new procedure to calculate the exchanged thermal power is established.

1. Introduction

In the next decades new projects involving the use of renewable energy sources will be needed to achieve a noticeable increase in energy production from renewable energy sources (RES) aimed at reducing carbon dioxide emissions and at meeting other targets, such as energy supply security. Every European country agreed to elaborate a National Renewable Energy Action Plan to reach the goal, as required by the EU (Directive 2009/28/EC, 2009).

In this context a clean, renewable and locally available thermal energy source can be provided by the use of energy geostructures. The multifunctional technology of energy tunnels represents an interesting alternative to traditional shallow geothermal technologies, well fitting in the context of an energy system transition that will bring important modifications to the way homes and other spaces will be heated and cooled. By thermally activating the structural elements of a construction in direct contact with the ground, a low enthalpy geothermal system can be achieved. This is obtained by embedding a circuit of pipes into the concrete members and by circulating a heat carrier fluid along it. This circuit is called the primary circuit and provides heat to a secondary circuit, that of the user. The connection among them can occur directly, as in the case of free heating and free cooling, or through a heat pump, allowing to vary the temperature to the necessary one. These energy geostructures can be used for heating and cooling of adjacent buildings and infrastructures, with a reduction of the initial installation costs, compared to conventional geothermal solutions (Boënnec, 2008; Adam and Markiewicz, 2009; Preene and Powrie, 2009; Bouazza et al., 2011; Barla et al., 2016).

In principle, all structures in contact with the ground can be used as energy geostructures (Brandl, 2006; Laloui and Di Donna, 2013; Pahud, 2013; Barla and Di Donna, 2016a; Soga and Rui, 2016). Piles, micropiles, diaphragm walls, anchors, tunnel linings can be mentioned among this technology. Recent studies focused on the application of this technology to tunnels (Barla and Perino, 2014a; Barla et al., 2015, 2016, 2017, 2019; Moormann et al., 2016; Bourne-Webb and da Costa Gonçalves, 2016; Bourne-Webb et al., 2016; Buhmann et al., 2016; Di Donna and Barla, 2016; Barla and Di Donna, 2018). In comparison with other energy

geostructures, energy tunnels are characterized by two main differences. Firstly, their much more extensive linear development implies a bigger surface in contact with the ground that could be thermally activated. Secondly, the tunnel's inner side lies in contact with the tunnel air, which could act as a source of heat in winter due to trains circulation. The fundamental three-fold role played by groundwater flow on the surrounding environment temperature, internal air distribution and on thermal performance and heat exchanger systems operation temperature was studied by many authors (Barla and Perino, 2014b, 2014c; Barla et al., 2016; Di Donna and Barla, 2016; Zhang et al., 2016; Bidarmaghz et al., 2017; Bidarmaghz and Narsilio, 2018). Nevertheless, the effect of groundwater flow direction cannot be found in any of these studies.

Barla and Di Donna (2016b) have proposed a novel segmental lining named Enertun which has been installed and tested by a real-scale energy tunnel prototype in the tunnel under construction of the Turin Metro Line 1 South Extension (Barla et al., 2019). The prototype allowed collecting a large amount of data on the thermal and structural performance of the lining.

Few studies have dealt with the thorough investigation of the thermal performance of energy tunnels based both on a monitored, full-scale site and on numerical results. It is the scope of this paper to analyse the original data collected for that pertaining to the thermal performance of the Enertun prototype in both the ground and the air configuration in order to investigate the energy efficiency of thermal activation of tunnels. Monitoring data allowed to calibrate a thermo-hydraulic numerical model and to reproduce the thermal performance in the conditions of the site. Corroboration of numerical models was not possible in previous literature for the Turin case given the unavailability of a testbed (Barla et al., 2014; Barla et al., 2016). Then, the calibrated parameters are used to generalise the results to different ground and environmental conditions, with particular reference to the still unstudied role of groundwater flow direction.

2. Experimental thermo-active tunnel prototype

In order to test the thermal performance of the newly patented energy segment, an experimental site of Enertun segmental lining was installed in the tunnel of Turin Metro Line 1 South Extension under construction, about 42 m northwards from Bengasi station, in the Lingotto-Bengasi section (Figure 1).

The experimental site is described in detail in Barla et al. (2019). Two rings of segmental lining were fully equipped with a total of 12 Enertun segments, for a total longitudinal length of 2.80 m. Two nets of pipes are included in the segments, one close to the extrados (tunnel surface in contact with the ground), the other close to the intrados (tunnel surface in contact with the air).

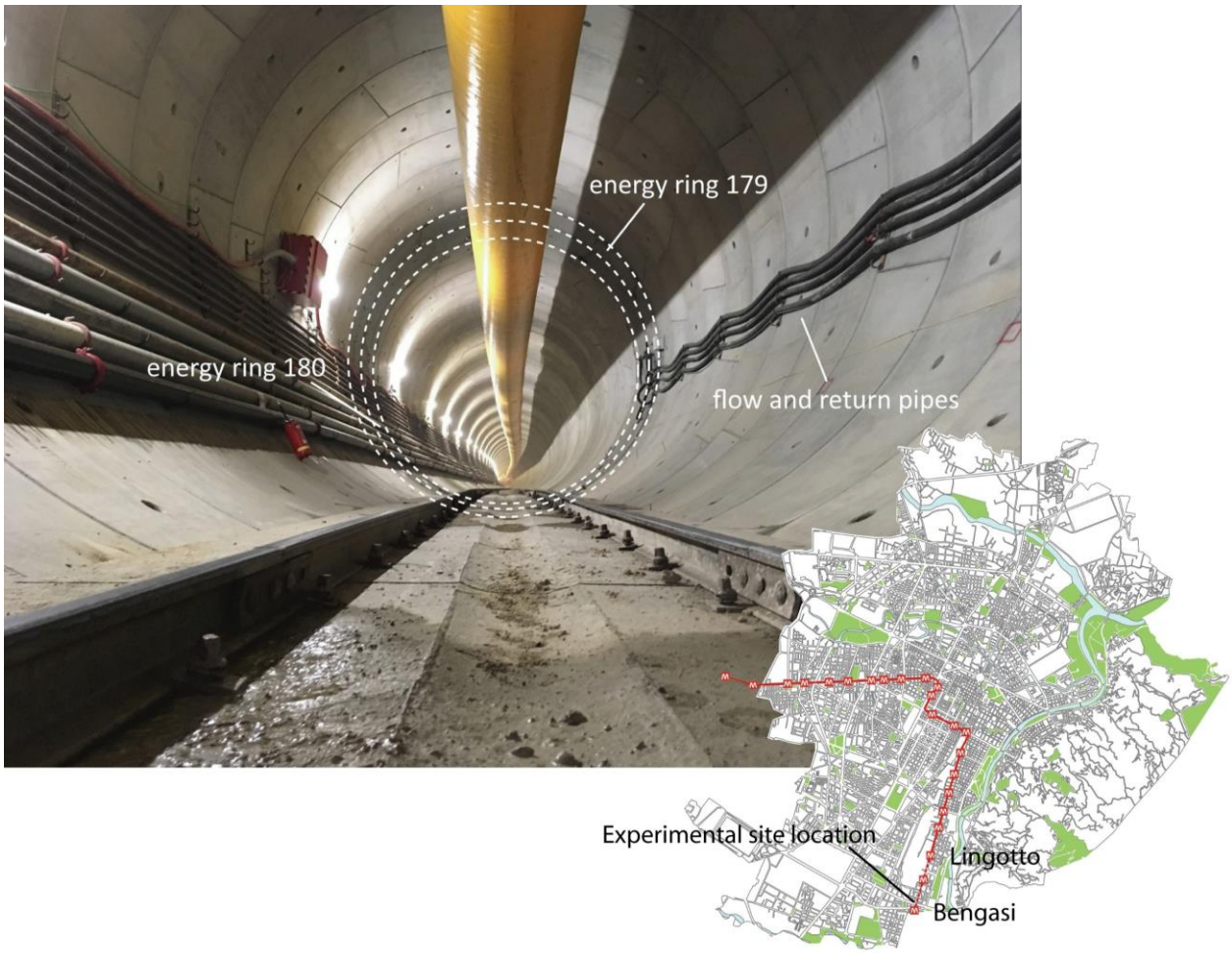

Figure 1. View of the Enertun experimental site and its location along the Turin Metro Line 1.

Energy rings were placed on site by the TBM at the beginning of July 2017 about 42 m from the entrance of the station. Installation chainage was decided in accordance with the construction site managers with the intention to minimize impact on the construction operations.

The Turin subsoil is constituted by glaciofluvial formations and hosts an unconfined aquifer (Barla and Barla, 2012). The geological profile in correspondence of the energy tunnel prototype (Figure 2) was obtained from the inspection of boreholes drilled ad hoc by the construction site along the line and by previous knowledge for the city of Turin (Barla and Barla, 2012). Below a shallow backfill layer, a sand and gravel unit from loose to weakly cemented (cementation included in the range 0-25%) can be highlighted. The tunnel is located within an aquifer, completely below the groundwater table surface whose depth oscillates between 11.7 and 12.4 m. Based on the data recorded by nearby piezometers, it is possible to detect a West-to-East groundwater flow and an hydraulic gradient in the range 0.3-0.5%.

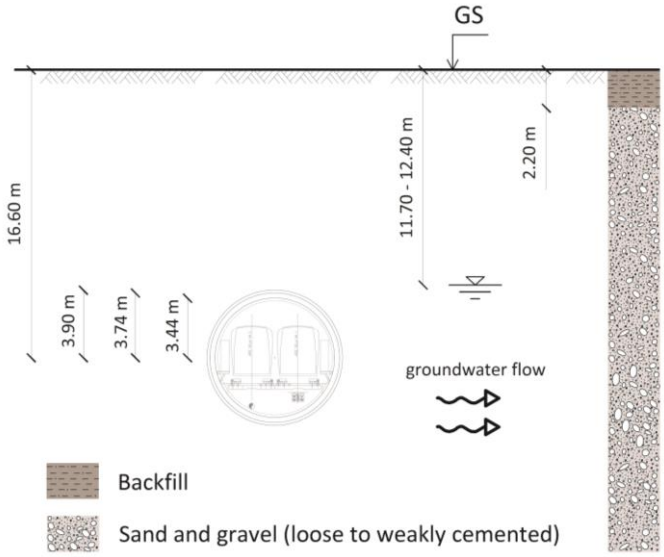

Figure 2. Hydrogeological cross section in correspondence of the energy tunnel prototype.

A heat pump device characterized by a useful thermal power in the range 4.8 and 7.4 kW was installed together with two hydraulic pumps that circulate the heat carrier fluid along the primary circuit. This fluid is a propylene glycol mixed with water allowing to work down to a temperature of −20 °C. Because of the experimental nature of the project, the secondary circuit of the heat pump is represented by a fan coil unit located close to the heat pump. Therefore, there were no real end users benefitting from the tests, but the heat was dissipated in or extracted from the air.

Given the complexity of the system to be investigated and the experimental nature of the project, a comprehensive monitoring system was installed to monitor the energy tunnel performance both from a thermal and a structural point of view (for the sake of brevity the drawings are not reported here, but the interested reader can refer to Barla et al. (2019)). The two energy rings were instrumented with a specifically designed monitoring system to observe stresses, strains and temperatures in the lining.

The aim of the experimental campaign was to evaluate efficiency and reliability of the prototype thermal activation together with its possible impacts on the lining. Monitoring started in September 2017 with the assessment of undisturbed conditions at the site. Differential stresses, differential strains and temperatures in the lining were recorded under natural fluctuations of tunnel air temperature (it has to be recalled that the site was still under construction, therefore external air temperatures are reflected in tunnel air).

The reversible heat pump made it possible to simulate summer and winter heating and cooling conditions. Depending on the fluid inlet temperature, this is warmed or cooled by the surrounding ground. During winter 2017/2018 heating mode tests were completed with both rings operating in parallel. At the end of each test the heat pump was turned off for long enough to ensure returning to the initial undisturbed thermal and mechanical conditions. Cooling mode test were performed during summer 2018. The total list of tests performed is given in Table 1, with 8 tests involving the ground circuit in heating mode (both continuous and cyclic), 2 tests where the ground circuit worked in cooling mode and 2 more tests where the air circuit was used to cool the tunnel air. Different volumetric flow rates and durations were chosen in order to collect a sound database for subsequent numerical back-analysis.

Table 1. List of the tests performed.

Test code	Circuit	Mode	Volumetric flow rate [m^3/h]	Fluid velocity [m/s]	Starting time [dd/mm/aa hh:mm]	Ending time [dd/mm/aa hh:mm]	Duration [d]

180215_G_H_T45_179180	Ground	Heating	1.3	0.90	15/02/2018 14:13	17/02/2018 09:57	1.82
180218_G_H_T45_179180	Ground	Heating	1.3	0.90	18/02/2018 13:57	20/02/2018 09:50	1.83
180222_G_H_T45_179180	Ground	Heating	1.3	0.90	22/02/2018 14:32	26/02/2018 12:50	3.93
180305_G_H_T45_179180	Ground	Heating	0.8	0.55	05/03/2018 14:05	07/03/2018 14:17	2.01
180309_G_H_T45_179180	Ground	Heating	1.0	0.69	09/03/2018 13:59	12/03/2018 15:47	3.07
180320_G_H_T45_179180	Ground	Heating	1.3	0.90	20/03/2018 14:00	28/03/2018 11:11	7.82
180407_G_H_T45_179180*	Ground	Heating	1.3	0.90	07/04/2018 10:00	16/04/2018 18:00	9.33
180508_G_H_T45_179180*	Ground	Heating	1.3	0.90	08/05/2018 10:04	20/05/2018 18:00	12.33
180727_G_C_T10_179180	Ground	Cooling	1.4	0.97	27/07/2018 11:29	30/07/2018 11:31	3.00
180801_A_H_T55_179180	Air	Heating**	1.3	0.90	01/08/2018 10:56	03/08/2018 15:56	2.21
180804_A_H_T55_179180	Air	Heating**	1.3	0.90	04/08/2018 20:00	06/08/2018 10:00	1.58
180807_G_C_T10_179180	Ground	Cooling	1.4	0.97	07/08/2018 12:22	09/08/2018 07:31	1.80

*Cyclic tests with heat pump on between 10:00 and 18:00.
**In this case the heat pump heating mode corresponds to tunnel cooling.

3. Energy performance of the prototype

The tests performed and listed in Table 1 allowed to investigate the energy performance of the experimental prototype of energy tunnel. The following considerations are then specifically referred to the conditions in which the prototype was tested, that is during the construction of the tunnel. Nevertheless, the data collected were particularly valuable to calibrate a thermo-hydraulic numerical model for the purpose of extending the discussion to other conditions (temperature boundary conditions, thermal ground properties, etc.), as debated in the following paragraphs.

For each test the inlet and outlet temperature over the whole duration were recorded by the heat pump. The procedure to evaluate the energy performance was as follows:

- The difference of temperature ΔT (in *°C*) between outlet and inlet was computed at any given time t_n when data were available

$$\Delta T(t_n) = |T_{outlet}(t_n) - T_{inlet}(t_n)| \quad (1)$$

- The heat flow, also called thermal power, $\Delta\dot{Q}$ (in *W* or *J/s*) was derived from the first law of thermodynamics, by computing the enthalpy flow $\Delta\dot{H}$ in the case of convective heat transfer, that is the main heat transfer mechanism taking place within the pipes

$$\Delta\dot{Q}(t_n) = \Delta\dot{H} = \dot{M} c_p \Delta T(t_n) \quad (2)$$

  where $\dot{M}$ is the mass flow rate expressed in *kg/s*, c_p is the specific heat capacity at constant pressure in *J/(kg·°C)* and ΔT is the temperature difference in *°C*

- The thermal energy extracted or injected for each timeframe $\Delta Q(t_n)$ (in *kWh*) was computed as the trapezoidal area under the curve $\Delta\dot{Q}(t)$

$$\Delta Q(t_n) = \frac{\left[\Delta\dot{Q}(t_n) + \Delta\dot{Q}(t_{n-1})\right] \cdot [t_n - t_{n-1}]}{2} \quad (3)$$

- The total energy extracted or injected during the test from the two energy rings was obtained by the following summation

$$Q = \sum_{t=t_{in}}^{t=t_{fin}} \Delta Q(t) \quad (4)$$

- The average thermal power $\dot{Q}$ was obtained by dividing the total energy extracted by the test duration. From $\dot{Q}$ it is possible to calculate the average thermal power extracted or injected per meter of tunnel lining or per square meter of tunnel lining by using the total longitudinal length of the prototype (2.8 m, in *W/m*) or its total contact surface area (65.8 m^2 for the ground circuit and 60.5 m^2 for the air circuit, in *W/m²*).

Table 2 summarizes the energy performance expressed in terms of thermal power (in W/m and in W/m^2) and of total thermal energy (in kWh) obtained for each of the tests listed in Table 1. It is pointed out that water, with 10% glycol was assumed in the computations, therefore c_p was equal to 4070 J/(kg·°C) and water density to 1009.6 kg/m^3.

Table 2. Energy performance of the prototype in terms of heat flux and thermal energy for each of the tests performed.

Test code	Thermal power		Thermal energy
	[W/m]	[W/m^2]	[kWh]
180215_G_H_T45_179180	1105	47.0	135.35
180218_G_H_T45_179180	1198	51.0	147.25
180222_G_H_T45_179180	1188	50.6	313.75
180305_G_H_T45_179180	959	40.8	129.44
180309_G_H_T45_179180	1076	45.8	222.34
180320_G_H_T45_179180	1135	48.3	601.12
180407_G_H_T45_179180	1198	51.0	250.50
180508_G_H_T45_179180	1233	52.5	340.64
180727_G_C_T10_179180	1421	60.5	286.59
180801_A_H_T55_179180	1142	52.8	169.47
180804_A_H_T55_179180	1179	54.6	125.48
180807_G_C_T10_179180	1559	66.4	86.85

Although the total number of tests is limited and do not allow for a statistical analysis, some additional considerations can be given by observing Figure 3a-c. From Figure 3a a nearly linear relationship between the volumetric flow rate of the fluid within the pipes and the heat flux is shown, that is heat flux increases with increasing flow rates. Heat fluxes between 41 and 53 W/m^2 were obtained considering both the continuous and the two cyclic tests. The energy performance was higher for ground cooling mode, mainly due to the higher flow rate and to the higher distance in temperature between the ground and the heat carrier fluid. When the air circuit was operated in tunnel cooling mode, heat flux values were similar to those of the ground heating and cooling tests. However, it has to be remarked that higher ranges of inlet and outlet temperatures occurred in this case, with a beneficial effect on the coefficient of performance of the heat pump.

In Figure 3b heat flux is plotted versus the test duration. No particular trends can be highlighted; therefore, the energy efficiency does not depend on the test duration and comparable thermal powers were obtained also in the case of longer tests, allegedly due to the favourable groundwater thermal recharge.

Figure 3c is intended to investigate any induced effect of the period of the year during which the test was carried out. The performance is seen only marginally affected leading to the convincement that it will be negligible during real operation of the tunnel, when the influence of external climatic conditions will be even lower than during the construction of the tunnel.

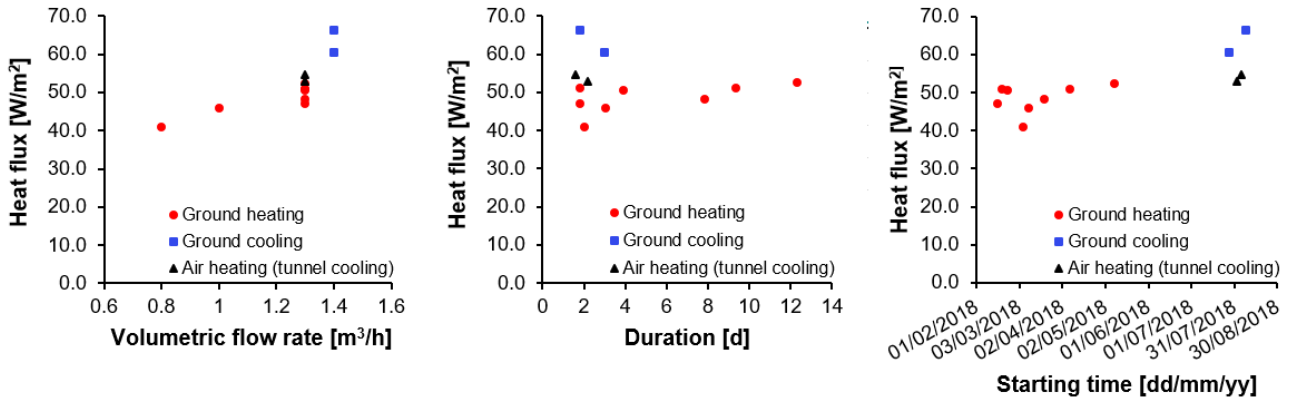

(a) (b) (c)

Figure 3. Energy tunnel thermal performance dependence on (a) heat carrier fluid volumetric flow rate, (b) test duration and (c) period of the year.

4. Numerical investigation of the thermal behavior of the prototype

The collection of experimental data concerning the real thermal behaviour of the energy tunnel prototype was used to draw some conclusions about its thermal performance. This is of particular relevance as no such results are available in literature for Italy and for hydrogeological conditions such as those existing in Turin. However, the conditions of the experimental campaign carried out are not fully representative of the general case of an operational tunnel, mainly because of the different temperature variations of the tunnel internal air. Nevertheless, this situation can be investigated by taking advantage of a three-dimensional, time-dependent, coupled thermo-hydraulic numerical model, that was first calibrated and then validated on the experimental results. This task is described in the following and is aimed at developing some updated design charts, in the path of the ones depicted in Di Donna and Barla (2016).

A 3D numerical model was built with the FEM software Feflow (Diersch, 2009) to reproduce the combined, transient thermo-hydraulic behaviour of the two Enertun rings installed in the experimental site. The TH problem is governed by mass conservation, energy conservation equations, and Darcy's velocity law, written in the Eulerian coordinate system for a saturated medium composed of a solid and a liquid (water) phase.
The model, whose cross section is shown in Figure 4, is 74.8 m high and 149.6 m wide, with a thickness of 8.4 m, for a total of 6 rings (the two middle rings are the energy rings). The external diameter of the tunnel is 7.48 m, with a 30 cm-thick concrete lining. An 11 cm-thick layer of grout all around the lining is also reproduced. A preliminary assessment of the appropriate boundary conditions to be adopted at the intrados of the tunnel to reproduce the influence of internal air was carried out. First, a 30-cm thick air layer was included in the model by assigning moving air thermal properties. Then, this layer was deactivated and a heat transfer boundary condition was applied, by computing the corresponding heat transfer coefficient. For the subsequent analyses the second boundary condition was adopted to reduce the total number of finite elements in the model.

The model is discretized into 2760016 triangular prismatic elements (49286 per layer) with 1420953 nodes (24929 per slice). The pipes, both ground-side and air-side, in the two equipped rings were accurately modelled reproducing the real geometry (segments rotated from one ring to another, asymmetric pipes layout along the longitudinal direction, segments different shapes and size) with one-dimensional elements, the so called "discrete features" (shown in blue in Figure 5), with a cross section area of 201 mm^2, corresponding to an external diameter of 20 mm and a thickness of 2 mm.

Both thermal and hydraulic boundary conditions were set. As shown in Figure 4, the initial temperature throughout the model was set at 17.3°C, as resulting from the interpolation of three measurements in the area of the experimental site (two piezometers and an extensometer well). The time series of the external air temperature was applied on the upper boundary of the model, which represents the free surface, whereas a constant value of 17.3°C was assigned to the lower boundary. On the tunnel internal boundary, the temperature was fixed following the data coming from the monitoring system. It should be remarked that the dual contact

of energy tunnel linings with the ground on one side and with the air on the other side is a peculiarity typical of tunnels and diaphragm walls. This is not an issue for energy piles, for example, and adds a degree of complexity and uncertainty to the boundary conditions that should be applied at the intrados to best recreate thermal conditions existing in situ. The hydraulic boundary conditions consist of a constant hydraulic head on the left and right sides, with different values on the two sides to allow a groundwater flow of 1.5 m/day from East to West and representative of a groundwater table depth of about 12.4 m at the tunnel centerline location, as measured in situ. Above the phreatic surface, air thermal properties were assigned.

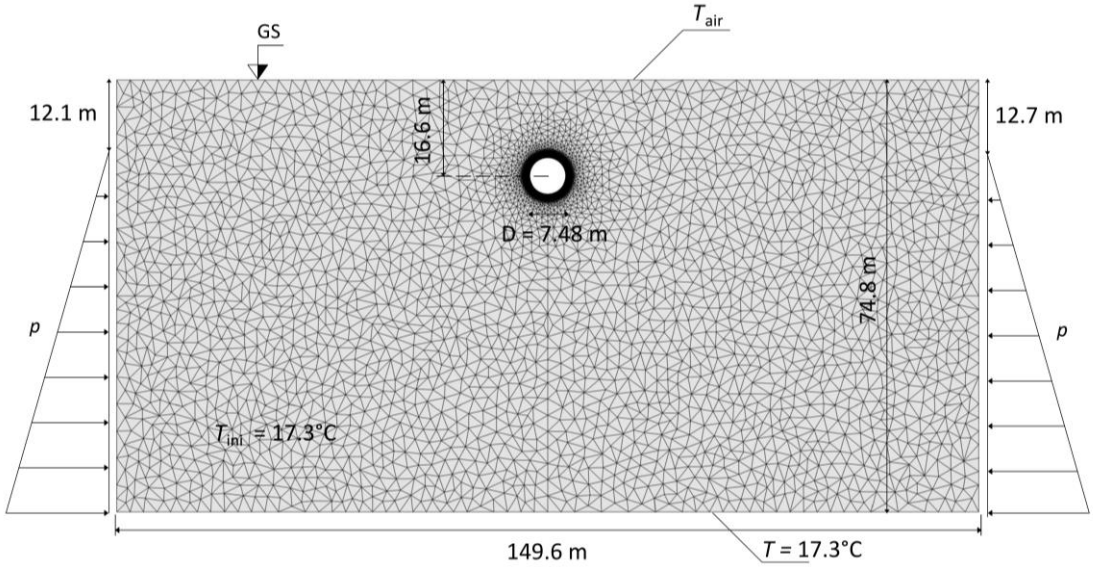

Figure 4. Cross section of the 3D FEM model with indication of thermal and hydraulic boundary conditions.

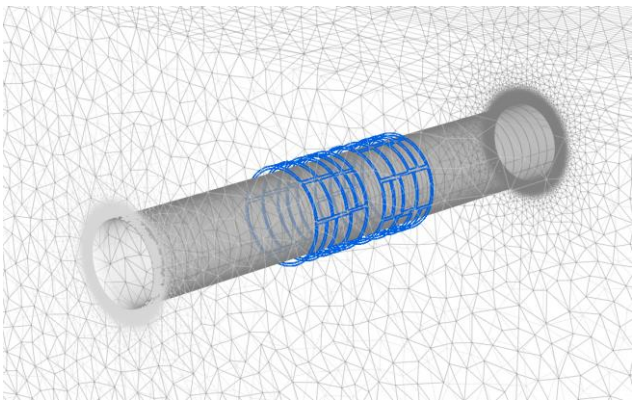

Figure 5. 3D view of the pipes circuit (expansion factor along longitudinal axis for a better view of the pipes network).

The numerical model was calibrated by considering the continuous ground heating mode test 180320_G_H_T45_179180, involving both rings working in parallel and characterized by a longer duration (see Table 1). To initialize the model and obtain a representative thermo-hydraulic state at the beginning of the test, a 30-days preliminary simulation was carried out with no thermal activation of the lining. At the end of this stage, a constant fluid velocity (0.9 m/s, Table 1) and a variable inlet temperature were imposed at the pipes inlets (velocity was also imposed at the outlets to keep it constant through the pipes), based on the monitoring data, for the whole length of the test.

First-trial hydraulic and thermal properties were obtained by previous studies (Barla et al., 2015, 2018), with the exception of the concrete thermal conductivity, which was obtained by means of hot guarded plate tests performed in the laboratory on the same concrete used for the precast Enertun segments. The calibration involved a number of trials. The values of a couple of thermal parameters, i.e. grout thermal conductivity and intrados heat transfer coefficient, were slightly modified, in the unavailability of any direct experimental

evaluation, until reaching a good superposition of simulation and monitoring outlet temperature. In particular, grout thermal conductivity was first assumed equal to the one for concrete and then reduced to 0.655 W/mK, as found by Allan and Kavanaugh (1999) for a cement & bentonite grout (the same grout composition adopted for Turin ML1 rings), to better fit experimental data. The adopted thermal conductivity value appears reasonable as no special mix design enhanced for thermal performance was adopted for the grout by the contractor. Material properties used in the numerical model are listed in Table 3 (note that blank cells mean that the same value as in Trial A was assumed), while Figure 6 exemplifies calibration results. The ground around the tunnel was assumed thermally isotropic and homogeneous.

Table 3. Material properties used during the calibration phase of the numerical model.

Material	Property	Symbol	Unit	Trial A	Trial B	Trial C
Ground	Horizontal hydraulic conductivity	K_{xx}, K_{zz}	m/s	4.150E-03		
	Vertical hydraulic conductivity	K_{yy}	m/s	2.075E-04		
	Specific storage	S_y	1/m	1.0E-04		
	Porosity	n	-	0.25		
	Fluid-phase thermal conductivity	λ_w	W/mK	0.65		
	Solid-phase thermal conductivity	λ_s	W/mK	2.8		
	Fluid-phase volumetric thermal capacity	$\rho_w c_w$	MJ/(m^{3}K)	4.2		
	Solid-phase volumetric thermal capacity	$\rho_s c_s$	MJ/(m^{3}K)	2		
	Transverse aquifer thermal dispersivity	α_T	m	0.31		
	Longitudinal aquifer thermal dispersivity	α_L	m	3.1		
Tunnel lining	Specific storage	S_y	1/m	1.0E-04		
	Solid-phase thermal conductivity	λ_s	W/mK	1.12		
	Solid-phase volumetric thermal capacity	$\rho_s c_s$	MJ/(m^{3}K)	2.19		
	Horizontal hydraulic conductivity	K_{xx}, K_{zz}	m/s	1.0E-16		
	Vertical hydraulic conductivity	K_{yy}	m/s	1.0E-16		
	Porosity	n	-	0		
	Transverse thermal dispersivity	α_T	m	0.5		
	Longitudinal thermal dispersivity	α_L	m	5		
Pipes	Specific storage	S_y	1/m	1.0E-04		
	Fluid-phase thermal conductivity	λ_w	W/mK	0.542		
	Fluid-phase volumetric thermal capacity	$\rho_w c_w$	MJ/(m^{3}K)	4.11		
	Longitudinal thermal dispersivity	α_L	m	5		
	Cross-sectional area	A	m^2	2.01E-04		
	Hydraulic aperture	b	m	0.8		
Grout	Specific storage	S_y	1/m	1.0E-04		
	Solid-phase thermal conductivity	λ_s	W/mK	1.12	0.655	0.655
	Solid-phase volumetric thermal capacity	$\rho_s c_s$	MJ/(m^{3}K)	2.19		
	Horizontal hydraulic conductivity	K_{xx}, K_{zz}	m/s	1.0E-16		
	Vertical hydraulic conductivity	K_{yy}	m/s	1.0E-16		
	Porosity	n	-	0		
	Transverse thermal dispersivity	α_T	m	0.5		
	Longitudinal thermal dispersivity	α_L	m	5		
Air layer	Heat transfer coefficient	Φ	W/m^{2}K	1.77	1.77	5.30

In Figure 6 it is possible to notice that the measured outlet temperature and the computed one are highly comparable, both in trial B and C, testifying a good calibration of the numerical model. However, trial C is the one that best fits also other tests, as demonstrated in Figure 7a-d that analyzes the results obtained during the validation phase for four more tests (two ground heating tests with different volumetric flow rates, one ground cooling test and one air heating test). The same procedure (30 days-initialization and test simulation) was followed also for the validation analyses. It is pointed out that a number of combinations of thermal and hydraulic parameters could yield a good match with the experimental outputs, but it stands to reason that the found set is fairly appropriate as comparison with a number of tests was undertaken.

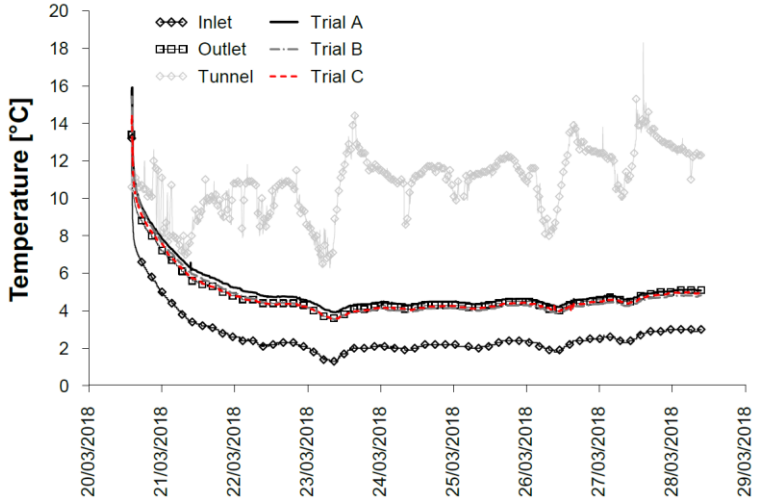

253
254 **Figure 6.** Comparison between measured and computed circuit outlet temperature: test 180320_G_H_T45_179180
255 (calibration phase).

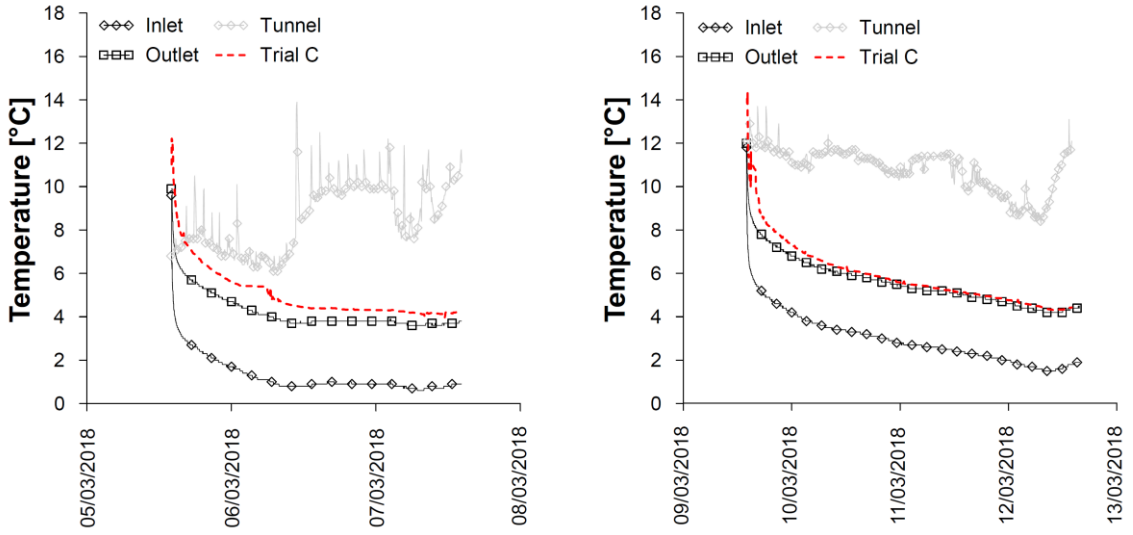

256

(a) (b)

257

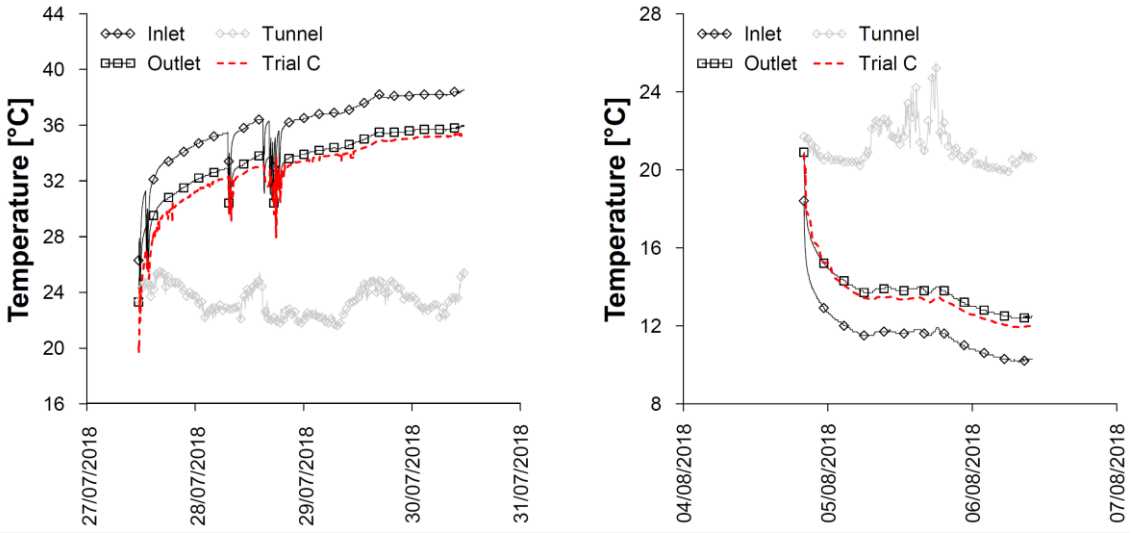

258

(c) (d)

259

Figure 7. Comparison between measured and computed data: (a) test 180305_G_H_T45_179180, (b) test 180309_G_H_T45_179180, (c) test 180727_G_C_T10_179180 and (d) 180804_A_H_T55_179180 (validation phase).

This is even more true noting that the temperatures computed numerically during the calibration phase, at four different locations in the lining, well reflect those measured by vibrating wire strain gauges at the intrados and at the extrados of the lining (see Figure 8a), considering that the embedded thermistor accuracy is 0.5°C.

Figure 8b depicts the computed downstream temperature from the tunnel lining intrados to the model right boundary at the end of the simulated tests, as well as the monitored temperature within the lining in correspondence of the location of three pairs of strain gauges with embedded thermistors (note that two different scales are used to better visualize the lining thermal profile and that the different background colours indicate the concrete layer, the grout layer and the ground; in Sl2i, Sl2e, St4i, St4e, St6i St6e *i* means intrados and *e* means extrados). A good match between computed and recorded results emerges. Moreover, it can be noted that for the test 180309_G_H_T45_179180 the thermal alteration is smaller than 1°C at 14 m distance, while it is even lower in the other tests. Unfortunately, monitoring data of surrounding rock temperature are not available. Indeed, during the design phase, it was ascertained that no downstream existing wells were available perpendicularly to the tunnel axis along the location of the energy tunnels. On the other hand, ad hoc wells could not be drilled for economic reasons as well as logistic constraints (the construction site is in the middle of a congestioned raods crossing).

According to the previous observations, the set of parameters C in Table 3 was adopted in the following.

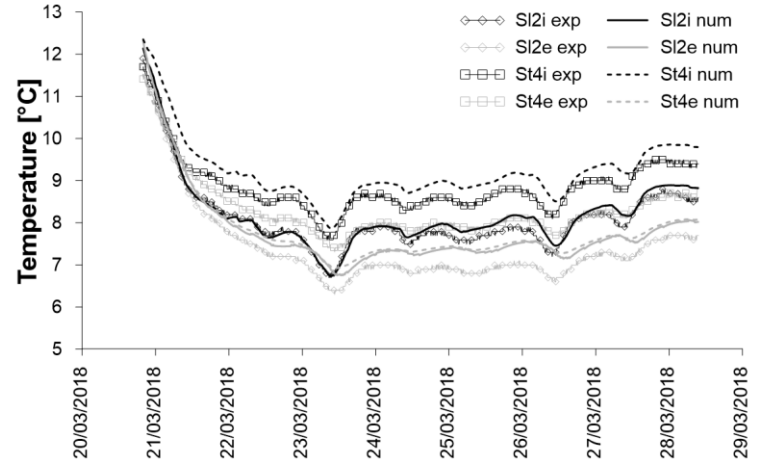

(a)

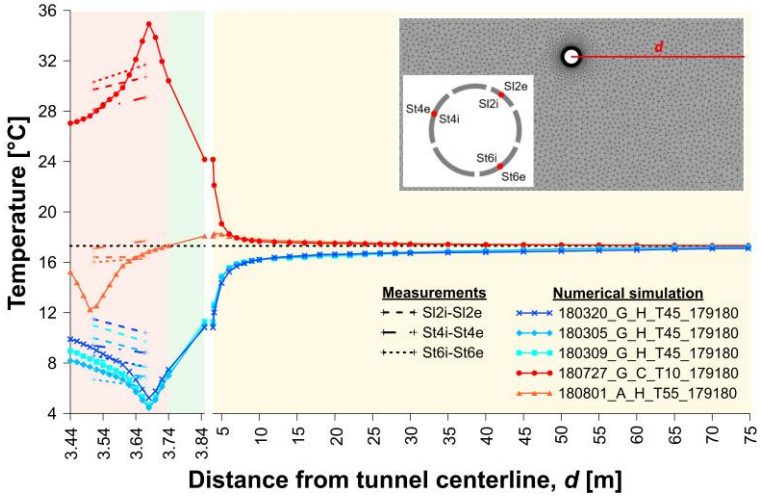

(b)

Figure 8. (a) Comparison between measured and computed lining temperature at the extrados and at the intrados: test 180320_G_H_T45_179180 (calibration phase); (b) Computed downstream temperature at the end of the simulated tests.

5. Generalization to different ground and environmental conditions

5.1. Developing design charts

The experimental data collected during the campaign accomplished in 2017-2018 along Turin ML1 South Extension were essential to demonstrate the robustness and reliability of the coupled numerical model. This had not been possible so far, which is why preliminary analyses had been described in literature. However, the feasibility and efficiency of energy tunnels could be legitimately argued when examining site-specific conditions different from that of the prototype described. To try to provide a comprehensive estimation of the thermal performance of the technology in a number of environmental situations, the design charts presented in Di Donna and Barla (2016), referred to previous configurations of the net of pipes, were updated for the Enertun scenario and for three different groundwater flow directions, that is parallel, forming an angle of 45° and running perpendicular to the tunnel axis. The analysis of the groundwater flow direction is an aspect of novelty in the framework of energy tunnels in comparison to previous literature. To this aim, a new thermo-hydraulic numerical model was built, made of 15 rings working in parallel and of six hypothetic energy segments of equal size (Figure 9). With special reference to the cases of parallel and oblique groundwater flow, results are pertaining to the eighth intermediate ring. The geometry of the tunnel is that of Turin ML1 SE. Of course, this could differ for other projects, but the size under study is quite representative of most typical urban tunneling situations. Further characteristics of the models are summarized in Table 4 (material properties not listed here can be found in Table 3). Temperature was fixed equal to the ground value at the top and bottom boundary, without considering the influence of atmospheric temperature oscillation. Different ground temperatures and corresponding tunnel temperatures were adopted to study various climatic conditions (Table 4). Average winter and summer temperatures measured in an already operational section of Turin Metro Line 1, that is 13.1 and 26.7°C respectively, were related to a ground temperature of 15°C. The seasonal analyses carried out involved 30 days of thermal initialization followed by 30 days of thermal activation. A sensitivity study was also performed by varying one by one fluid inlet temperature, fluid velocity, pipes size and heat transfer coefficient at the intrados elements.

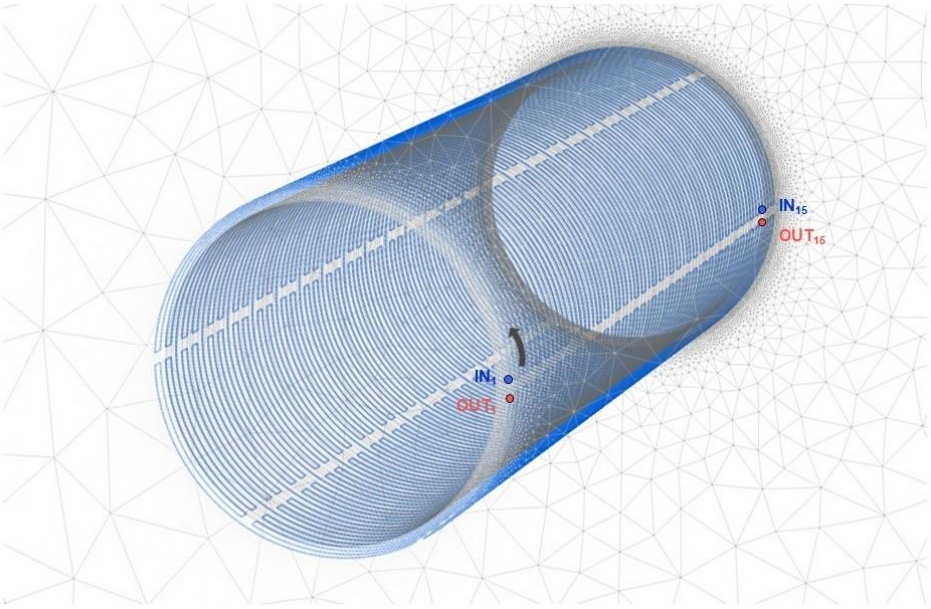

Figure 9. Geometry of the network of pipes embedded in the model adopted for the construction of design charts (only inlets and outlets of rings 1 and 15 are highlighted for illustrative purposes).

Table 4. Main properties of the base and sensitivity analyses models

Characteristic	Unit	Value
Pipes size	mm	20x2
Inlet temperature (winter)	°C	4
Inlet temperature (summer)	°C	28

Heat carrier fluid velocity	m/s	0.9
Grout thermal conductivity	W/mK	2
Concrete thermal conductivity	W/mK	1.5
Grout thickness	cm	11
Ground temperature	°C	9-12-15-18
Heat transfer coefficient	W/(m^{2}K)	5.3
Tunnel temperature (winter)	°C	Variable with ground temperature 7.1-10.1-13.1-16.1
Tunnel temperature (summer)	°C	Variable with ground temperature 20.7-23.7-26.7-29.7
Ground thermal conductivity	W/mk	0.9-2.26-3.9
Groundwater flow	m/d	0-0.5-1-1.5-2

The resulting design charts can be seen in Figure 10 for winter and summer modes and for different groundwater flow directions with respect to the tunnel axis. With different colors the ranges of thermal flux in W/m^2 are indicated for each triplet of ground temperature, groundwater flow velocity and ground total thermal conductivity. The analyses were carried out for specific triplets, organized on a grid, and then interpolated by using an appropriate polynomial law able to match satisfactorily the discrete, scattered numerical results. The charts related to the case of perpendicular flow are in line with the existing ones, although a one-to-one quantitative comparison is not possible due to different model inputs (presence of grout, different concrete thermal conductivity, pipes size, heat carrier fluid velocity, intrados boundary condition). Considerations drawn by Di Donna and Barla (2016) are confirmed here. No matter the flow direction, the highest performance is obtained with maximum ground thermal conductivity, maximum groundwater flow, due to the thermal recharge mechanism that allows the ground to return more rapidly to its undisturbed temperature, and with maximum ground temperature in winter and vice versa in summer. As groundwater flow velocity decreases, thermal conductivity starts playing a role, since the dotted and dashed lines representing boundaries between heat flux ranges move away from the continuous ones. For perpendicular groundwater flow winter energy performance is in the range 10-95 W/m^2, while summer energy performance falls between 10-110 W/m^2., slightly higher than in summer. By observing the effect of groundwater flow, it is possible to notice that a substantial increase in performance occurs when going from 0° to 45°, whereas little improvement is attributable to perpendicular flow in comparison to the oblique case. It is reasonable to think that thermal performance does not increase linearly with increasing groundwater tilt angle, but with a gradually decreasing gradient.

Winter – heat extraction

Summer – heat injection

0°

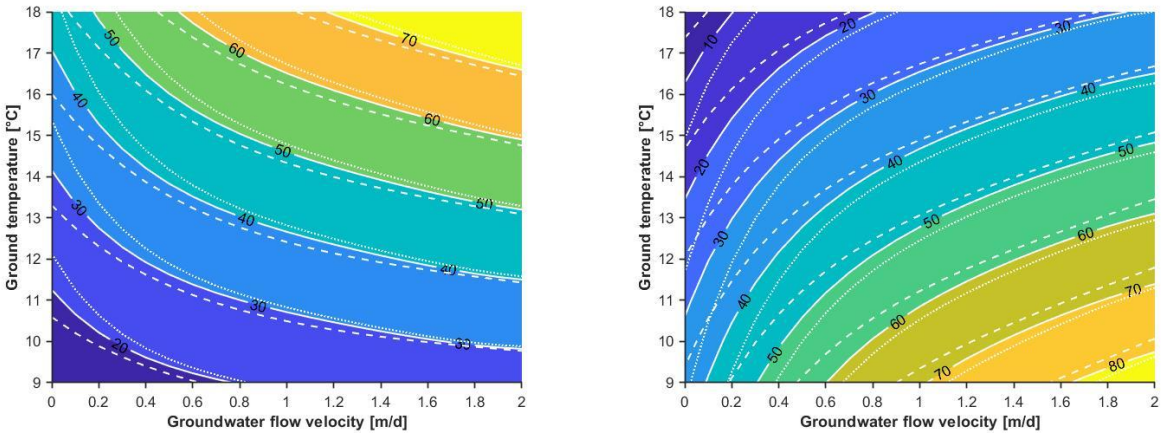

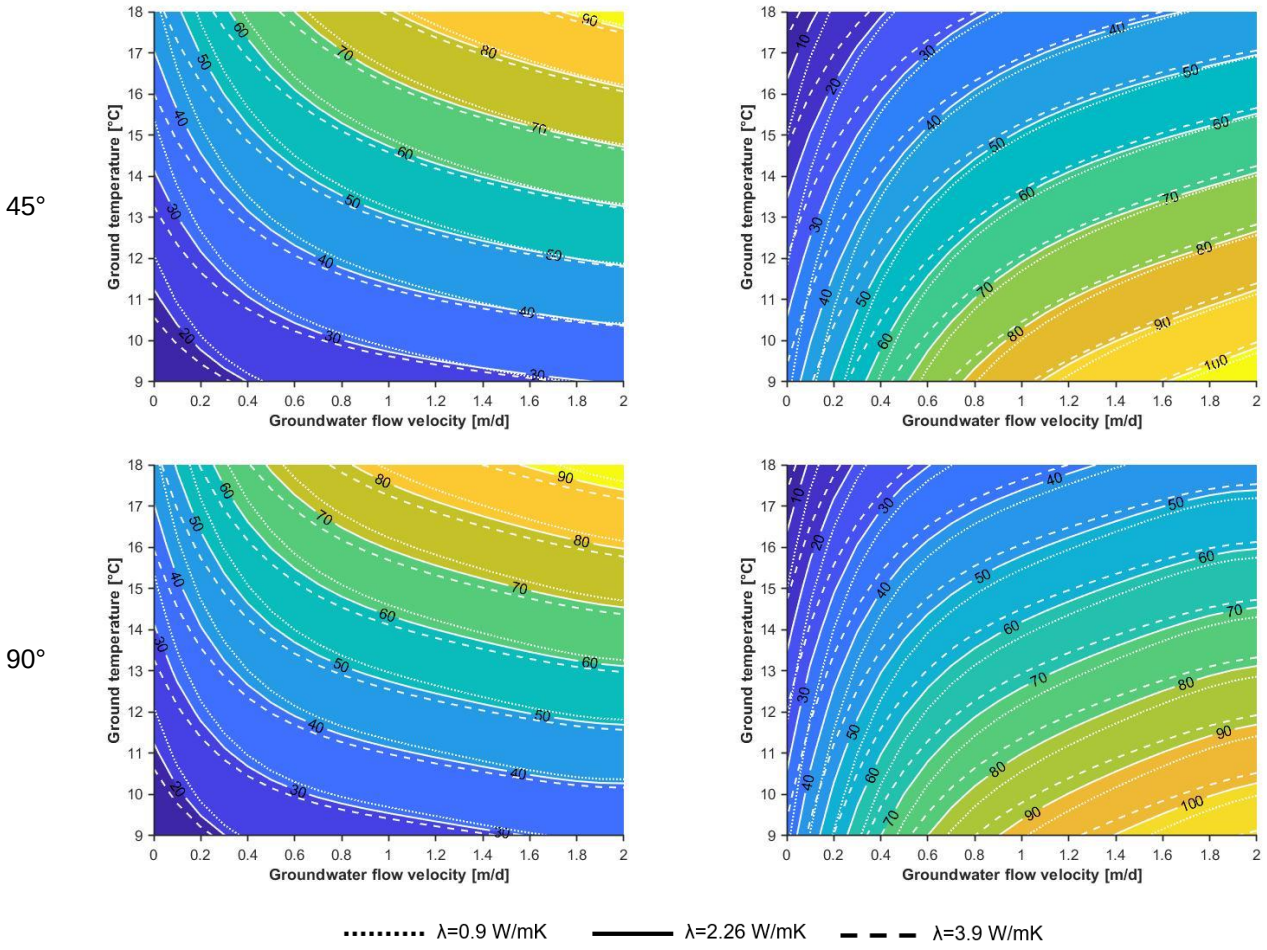

Figure 10. Updated preliminary design charts showing geothermal potential in W/m^2 for winter and summer conditions and for different groundwater flow directions with respect to the tunnel axis (0°, 45° and 90°).

These charts are particularly useful for the designer interested in evaluating whether it may be worth or not to invest in the feasibility study of the thermal activation of a tunnel. It is clear that a more detailed study should be conducted at the design analysis stage, as described for example in Barla and Di Donna (2018) and Baralis et al. (2018).

5.2. Sensitivity analyses

To investigate the validity and range of application of the design charts, it is of interest to assess the effect of other possibly varying design parameters on thermal efficiency. For this reason, some sensitivity analyses were carried out to explore the influence of different values of fluid inlet temperature T_{in}, fluid velocity v_f, pipes size d,t (diameter and thickness) and heat transfer coefficient Φ, as shown in Table 5.

Table 5. Parameters investigated in the sensitivity analyses.

Design parameter	Unit	Values	
$T_{in,winter}$	°C	1	7
$T_{in,summer}$	°C	32	36
v_f	m/s	0.4	1.4
d x t	mm	16x2	25x2.3
Φ	W/m^{2}K	1	15

The range of variation of the heat transfer coefficient was based on the table reported in Di Donna et al. (2016). The analyses were conducted for six relevant combinations of groundwater flow velocity and ground

temperature (ground thermal conductivity kept to 2.26 W/mK) so that all the chart area is spanned. In the following each aspect is explored and commented in detail.

Fluid inlet temperature. The paramount importance of fluid inlet temperature emerges clearly in Figure 11a in comparison to the other investigated aspects (it is highlighted that in this chart the range is two times that of the other charts) as it highly affects heat transfer, with variations of the heat flux reaching 56 W/m^2 in summer when using the highest inlet temperature. This parameter appears to be strictly dependent on groundwater flow velocity, as the mechanism of thermal recharge avoids heating or cooling of the surrounding ground thus improving thermal performance.

Fluid velocity and pipes size. It can be seen from Figure 11b that the minimum variation in the heat flux occurs when thermal exchange is minimum (low groundwater flow and low ground temperature in winter, low groundwater flow and high ground temperature in summer), whereas the maximum variation occurs in the opposite case. This last is not negligible, hence care should be taken when falling in this area (upper right and lower right corner of the design chart in winter and summer, respectively). The same goes when assessing the effect of pipes dimension (Figure 11c), although the maximum variations are lower than in the previous case.

Heat transfer coefficient. Quite different is the case of sensitivity analyses on the heat transfer coefficient value (Figure 11d). This coefficient has an effect on the amount of heat flowing from/to the tunnel environment to/from the lining. When the heat transfer coefficient is 15 W/m^{2}K, the heat flux increases by a maximum of 14 W/m^2 in winter and by 8 W/m^2 (or decreases by 4 W/m^2) in summer. When the heat transfer coefficient is 1 W/m^{2}K, the heat flux decreases by a maximum of 19 W/m^2 in winter and by 10 W/m^2 (or increases by 5 W/m^2) in summer. The overall ranges of variation are not too different from that of fluid velocity and pipes size.

The results obtained above, considering a perpendicular groundwater flow, were confirmed by running a number of relevant analyses for oblique and parallel flow.

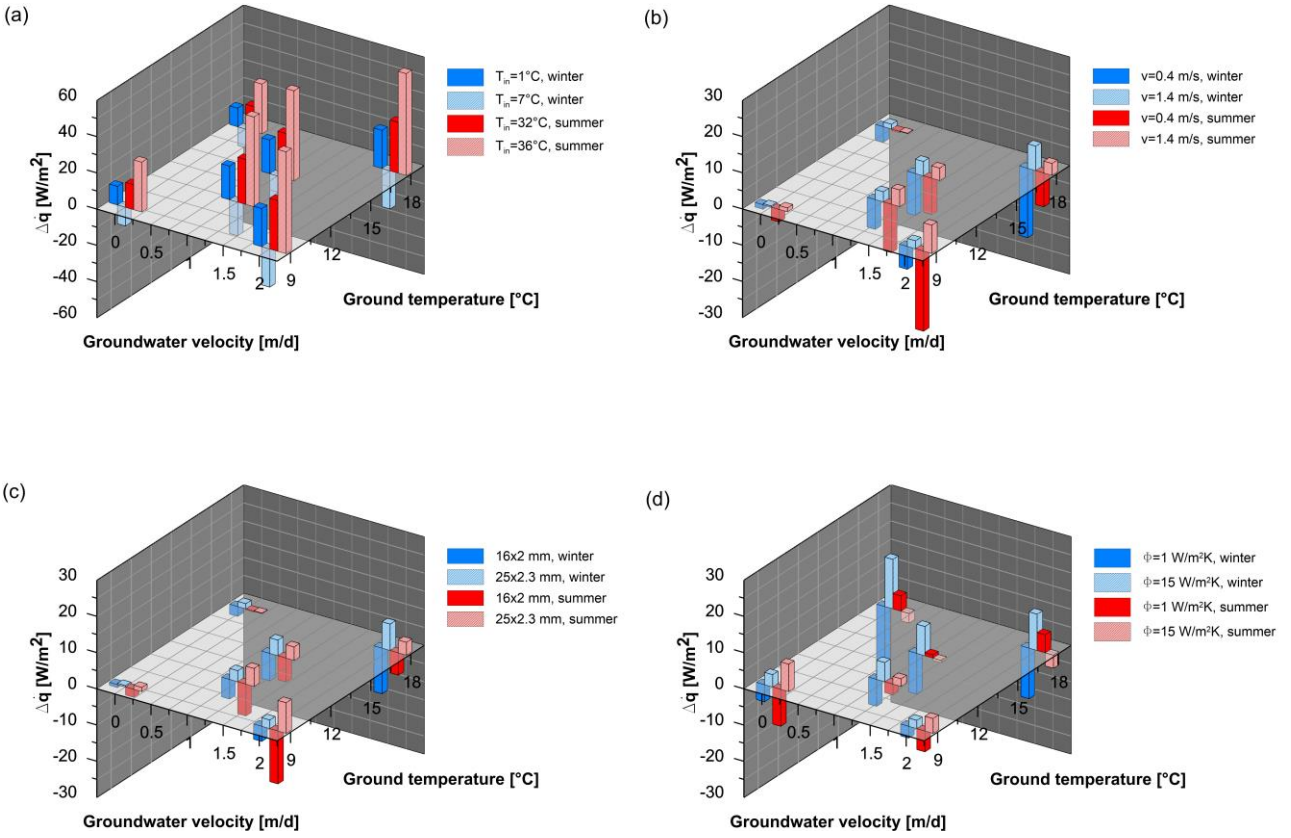

Figure 11. Effect of (a) fluid inlet temperature, (b) fluid velocity, (c) pipes size and (d) heat transfer coefficient on geothermal potential during winter and summer conditions expressed in terms of heat flux variations in the case perpendicular flow.

Based on the sensitivity analyses one can conclude that fluid inlet temperature is the parameter that mostly affects heat transfer. Hence, to evaluate geothermal potential the following procedure can be followed:

- assess local groundwater flow direction and choose the appropriate chart;
- assess local groundwater flow velocity, ground undisturbed temperature and thermal conductivity;
- based on the previous inputs, evaluate the exchangeable heat $\dot{q}^*$ from the design chart;
- if an inlet temperature different from 4°C in winter and 28°C in summer is expected, correct $\dot{q}^*$ based on the following relationship

$$\dot{q} = \dot{q}^* + \Delta\dot{q} \tag{5}$$

with

$$\Delta\dot{q}/\Delta T = 3.44 - \frac{{v_{gw}}^{2.01}}{3.09} + 4.44 * ln(1 + v_{gw}) \quad \text{in summer} \tag{6}$$

$$\Delta\dot{q}/\Delta T = -\left[3.44 - \frac{{v_{gw}}^{2.01}}{3.09} + 4.44 * ln(1 + v_{gw})\right] \quad \text{in winter} \tag{7}$$

in the case of perpendicular and oblique groundwater and

$$\Delta\dot{q}/\Delta T = 3.44 - \frac{{v_{gw}}^{0.74}}{3.05} + 2.75 * ln(1 + v_{gw}) \quad \text{in summer} \tag{8}$$

$$\Delta\dot{q}/\Delta T = -\left[3.44 - \frac{{v_{gw}}^{0.74}}{3.05} + 2.75 * ln(1 + v_{gw})\right] \quad \text{in winter} \tag{9}$$

in the case of parallel groundwater, where ΔT is the difference between the actual inlet temperature and the theoretical one (4 or 28°C depending on the season) and v_{gw} is the groundwater flow velocity expressed in m/d. The equations above were obtained by direct interpolation of the computed data.

- consider a ±10 W/m^2 correction to the above obtained value of W/m^2 to take into account different fluid velocity, pipes size and heat transfer coefficient.

Considering all the above, the design charts can be reliably adopted for a wide range of conditions. Having said this, it is clear that they cannot be considered as a general and unique indication for the evaluation of the geothermal potential of an energy tunnel and that a more detailed study should be conducted at the design analysis stage, by site-specific thermo-hydraulic numerical modelling that include detailed aspects of ground conditions, site installation and working conditions.
As an example, aspects such as the intermittent ratio (i.e. the ratio of interval time to running time as defined by Ogunleye et al. (2020) and Zhang et al. (2014)) are not explicitly taken into account in the parametric design charts, especially for the cases of slow or absent groundwater flow. For the cases with a major groundwater flow, the intermittent ratio is not expected to play a relevant role. Instead, when no groundwater flow is present at the site, it could be crucial in assessing the feasibility of an energy tunnel project. Specific thermo-hydraulic analyses should be performed at a later design stage to find an optimization strategy of the intermittent ratio so that the geothermal resource is not depleted and is properly used. Similarly, different tunnel climates arising from particular operation conditions (e.g. “hot” tunnels) should be specifically analyzed. Moreover, as winter and summer cases are considered separately, thus leading to two seasonal design charts, possible unbalanced heat situations do not emerge and cannot be catched. Long-term yearly analyses should be performed to assess this issue, both in the case of heating only, cooling only or heating and cooling (this is particularly true for

unfavourable hydrogeological conditions and for single-mode operation, i.e. continuous heating only or cooling only).

6. Validation against existing data

The design charts here presented were validated against available literature data. A summary of the obtained results can be observed in Table 6. A very good match is obtained in most of the cases with the actual values falling within the ranges anticipated by the design charts. This applies to cases based on numerical studies as well as to real monitored data.

Smaller values are shown for the Grand Paris Express B with respect to the computed ones. Here Cousin et al. (2019) have considered a tunnel temperature as high as 18.96°C and a heat transfer coefficient of 15.13 W/m^2K which certainly has a positive effect on the heat exchange. It is noted that this also leads to substantially different results from those reported in Bracq et al. (2017) and Fouché et al. (2018) for a similar case study. Minor difference is also shown for the case of Warsaw NE metro. However, in this case the Authors have considered adiabatic boundary conditions in the tunnel.

The case of Turin ML1 is shown to be slightly more favourable when using the design charts than in the previous study performed by Di Donna and Barla (2016) and Barla et al. (2016). The reason lies on the fact that the more efficient Enertun configuration has been used here.

Table 6. Validation of the design charts against available data of energy tunnels thermal power exchanged with the ground.

Case study	R/N*	v_{gw} [m/d]	T_g [°C]	λ [W/mK]	q [W/m²]			
					Result of the study		Design charts	
					Winter	Summer	Winter	Summer
Crossrail (Nicholson et al., 2013, 2014)	N	0	14.8	1.8	10-30	-	22-42	-
Grand Paris Express A (Bracq et al., 2017; Fouché et al., 2018)	N	0	12	1.6-2.4	15-30	10-20	13-33	15-35
Grand Paris Express B – case 2.1 (Cousin et al., 2019)	N	0	13	2.1-2.3	50	-	24-44	-
Jenbach (Frodl et al., 2010; Mayer and Franzius, 2010; Franzius and Pralle, 2011; Buhmann et al., 2016; Moormann et al., 2016)	R	1	10	3.3	18-40	-	18-38	-
Katzenbergtunnel (Franzius and Pralle, 2011)	R	0	13	3	17-25	-	19-39	-
Turin ML1 SE (Di Donna and Barla, 2015; Barla and Di Donna, 2016b, 2018; Barla et al., 2016)	N	1.5	14	2.26	53	74	53-73	58-78
Warsaw NE metro - model 1 (Baralis et al., 2018)	N	0	12	1.61	13	30	11-31	10-30
Warsaw NE metro - model 2 (Baralis et al., 2018)	N	0.09	12	2.40	15	42	17-37	19-39

*R=real case study N=numerical study

7. Conclusions

A comprehensive study on the energy performance of energy tunnels was carried out with the aim of providing quick and effective tools to designers who want to quantify heat exchange in a preliminary phase of the project. The main conclusions are as follows:

- Thanks to a real scale prototype constituted by a pair of energy rings Enertun-type recently tested for the first time in Italy, an experimental campaign allowed to assess the thermal performance of tunnels in a variety of conditions (different durations and flow rates, heating case, cooling case). From the processing of data collected, it was possible to infer that winter extraction thermal power amounts to 47-52.5 W/m^2, while in summer a range of 60.5-66.4 was obtained. Despite the longest test lasted more than 12 days, long-term tests are not available yet but are planned to be performed during tunnel operation.
- A 3D time-dependent thermo-hydraulic numerical model was calibrated and validated on the monitored data pertaining to the two experimental Enertun rings so that it was proved to be able to adequately simulate the conditions existing in situ. With respect to previous studies, consideration of a grout layer was included whose thermal conductivity was calibrated ad hoc. Heat transfer coefficient was also deduced by matching local temperatures measured in the lining and resulted to be slightly higher than the one used in previous models referred to the Turin case.
- The system operational behaviour was investigated in conditions different from the tested ones to generalise the results. Design charts were presented with the intention of updating to the Enertun layout those already existing in literature. In this new version, different groundwater flow directions as well as the influence of fluid inlet temperature, fluid velocity, pipes size and heat transfer coefficient were also considered. A substantial increase in performance occurs when water flow direction increases from 0° to 45°, whereas little improvement is attributable to perpendicular flow in comparison to the oblique case. The paramount importance of fluid inlet temperature emerges in comparison to the other investigated aspects.
- A new simplified procedure to calculate the exchanged thermal power by using the design charts was suggested. It can be reliably adopted for a preliminary evaluation in a wide range of conditions. It is clear, however, that a more detailed study should be conducted at the design analysis stage, which includes site-specific thermo-hydraulic numerical modelling, and that caution should be adopted when site conditions differ substantially from those considered in the sensitivity analysis herewith described.

Acknowledgements

The Authors are willing to acknowledge Prof. Marco Zerbinatti and Lorenzo Salomone (from the Department of Structural, Building and Geotechnical Engineering) and Stefano Fantucci (from the Energy Department of Politecnico di Torino) for carrying out hot guarded plate tests aimed at evaluating the segments concrete thermal conductivity. The Authors are thankful to the help of the large number of people and companies that, in different ways, contributed to accomplish the installation of the first prototype of energy tunnel in Italy as the result of an agreement set by the Politecnico di Torino, InfraTo, the owner, and Consorzio Integra, the contractor. In this respect, special thanks are devoted to Vanni Cappellato, Roberto Crova and Giovanni Currado (from InfraTo), Guido Bay and Lorenzo Fiorentino (from CMC). Particular thanks is also devoted to Stefania Di Giovanni (from CMC) for the hints and suggestions provided on technical issues and details.

References

Adam, D., Markiewicz, R., 2009. Energy from earth-coupled structures, foundations, tunnels and sewers. Géotechnique 59, 229–236. https://doi.org/10.1680/geot.2009.59.3.229

Allan, M.L., Kavanaugh, S.P., 1999. Thermal Conductivity of Cementitious Grouts and Impact On Heat Exchanger Length Design for Ground Source Heat Pumps Thermal Conductivity of Cementitious Grouts and Impact On Heat Exchanger Length Design for Ground Source Heat Pumps. HVAC&R Res. 85–96. https://doi.org/10.1080/10789669.1999.10391226

Baralis, M., Barla, M., Bogusz, W., Di Donna, A., Ryzynski, G., Zerun, M., 2018. Geothermal Potential of the NE Extension Warsaw Metro Tunnels. Environ. Geotech. https://doi.org/https://doi.org/10.1680/jenge.18.00042

Barla, G., Barla, M., Bonini, D.M., Debernardi, D., Perino, A., Antolini, F., Gilardi, M., 2015. 3D thermo-hydro modeling and real-time monitoring

for a geothermal system in Torino, Italy, in: Geotechnical Engineering for Infrastructure and Development ICE Publishing XVI ECSMGE, Edinburgh 13-17 September 2015. pp. 2481–2486. https://doi.org/10.1680/ecsmge.60678

Barla, M., Barla, G., 2012. Torino subsoil characterization by combining site investigations and numerical modelling. Geomech. Tunn. 5, 214–231.

Barla, M., Di Donna, A., 2016a. Editorial Themed issue on energy geostructures. Environ. Geotech. 3, 188–189.

Barla, M., Di Donna, A., 2016b. Conci energetici per il rivestimento delle gallerie. STRADE & AUTOSTRADE 5, 2–5.

Barla, M., Di Donna, A., 2018. Energy tunnels: concept and design aspects. Undergr. Sp. https://doi.org/10.1016/j.undsp.2018.03.003

Barla, M., Di Donna, A., Baralis, M., 2018. City-scale analysis of subsoil thermal conditions due to geothermal exploitation. Environ. Geotech. 1–11.

Barla, M., Di Donna, A., Insana, A., 2017. Energy Tunnel Experimental Site in Turin Metro, in: 15th IACMAG. Wuhan, China.

Barla, M., Di Donna, A., Insana, A., 2019. A novel real-scale experimental prototype of energy tunnel. Tunn. Undergr. Sp. Technol. 87, 1–14.

Barla, M., Di Donna, A., Perino, A., 2016. Application of energy tunnels to an urban environment. Geothermics 61, 104–113. https://doi.org/10.1016/j.geothermics.2016.01.014

Barla, M., Perino, A., 2014a. Energy from geo-structures: a topic of growing interest. Environ. Geotech. 2, 3–7. https://doi.org/10.1680/envgeo.13.00106

Barla, M., Perino, A., 2014b. Energy from geo-structures: a topic of growing interest. Environ. Geotech. 2, 3–7. https://doi.org/10.1680/envgeo.13.00106

Barla, M., Perino, A., 2014c. Geothermal heat from the Turin metro south extension tunnels. Proc. World Tunn. Congr. 2014 Tunnels a better life.

Bidarmaghz, A., Narsilio, G.A., 2018. Heat exchange mechanisms in energy tunnel systems. Geomech. Energy Environ. https://doi.org/10.1016/j.gete.2018.07.004

Bidarmaghz, A., Narsilio, G.A., Buhmann, P., Moormann, C., Westrich, B., 2017. Thermal interaction between tunnel ground heat exchangers and borehole heat exchangers. Geomech. Energy Environ. 10, 29–41. https://doi.org/10.1016/j.gete.2017.05.001

Boënnec, O., 2008. Shallow ground energy systems. Proc. Inst. Civ. Eng. - Energy 161, 57–61. https://doi.org/10.1680/ener.2008.161.2.57

Bouazza, A., Adam, D., Rao Singh, M., Ranjith, P.G., 2011. Direct Geothermal Energy from Geostructures. Aust. Geotherm. Energy Conf. 2011 21–24.

Bourne-Webb, P., da Costa Gonçalves, R., 2016. On the Exploitation of Ground Heat Using Transportation Infrastructure, in: Procedia Engineering. Elsevier B.V., pp. 1333–1340. https://doi.org/10.1016/j.proeng.2016.06.157

Bourne-Webb, P.J., Bodas Freitas, T.M., Da Costa Gonçalves, R.A., 2016. Thermal and mechanical aspects of the response of embedded retaining walls used as shallow geothermal heat exchangers. Energy Build. 125, 130–141. https://doi.org/10.1016/j.enbuild.2016.04.075

Bracq, G., Soussi, C., Fouché, O., Minec, S., 2017. Utilisation de l'énergie géothermique en tunnel/Capturing geothermal energy using tunnel lining, in: Congrès International de l'AFTES - L'espace Souterrain Notre Richesse. pp. 1–8.

Brandl, H., 2006. Energy foundations and other thermo-active ground structures. Géotechnique 56, 81–122. https://doi.org/10.1680/geot.2006.56.2.81

Buhmann, P., Westrich, B., Moormann, C., Bidarmaghz, A., Narsilio, G., 2016. An investigation of the potential thermal energy of geothermal tunnels with focus on a case study in Stuttgart, Germany. Energy Geotech. - Proc. 1st Int. Conf. Energy Geotech. ICEGT 2016.

Cousin, B., Rotta, A.F., Bourget, A., Rognon, F., Laloui, L., 2019. Energy performance and economic feasibility of energy segmental linings for subway tunnels. Tunn. Undergr. Sp. Technol. 91, 102997. https://doi.org/10.1016/j.tust.2019.102997

Di Donna, A., Barla, M., 2015. The role of ground conditions and properties on the efficiency of energy tunnels. Environ. Geotech. https://doi.org/10.1680/jenge.15.00030

Di Donna, A., Barla, M., 2016. The role of ground conditions and properties on the efficiency of energy tunnels. Environ. Geotech. 3.

Di Donna, A., Cecinato, F., Loveridge, F., Barla, M., 2016. Energy performance of diaphragm walls used as heat exchangers. Proc. Inst. Civ. Eng. - Geotech. Eng. 1–14. https://doi.org/10.1680/jgeen

Diersch, H.J.G., 2009. DHI wasy software – Feflow 6.1 – Finite element subsurface flow & transport simulation system: Reference manual.

Directive 2009/28/EC, 2009. Directive 2009/28/EC of the European Parliament and of the Council of 23 April 2009. Off. J. Eur. Union 140, 16–62. https://doi.org/10.3000/17252555.L_2009.140.eng

Fouché, O., Soussi, C., Bracq, G., Minec, S., 2018. Seasonal storage of sensible heat in tunnel-surrounding rocks, in: Proceedings of the First International Conference on Advances in Rock Mechanics, TUNIROCK 2018, Hammamet, Tunisia, 29-31 March 2018. pp. 63–68.

Franzius, J.N., Pralle, N., 2011. Turning segmental tunnels into sources of renewable energy. Proc. ICE - Civ. Eng. 164, 35–40. https://doi.org/10.1680/cien.2011.164.1.35

Frodl, S., Franzius, J.N., Bartl, T., 2010. Design and construction of the tunnel geothermal system in Jenbach / Planung und Bau der Tunnel-Geothermieanlage in Jenbach. Geomech. Tunn. 3, 658–668. https://doi.org/10.1002/geot.201000037

Laloui, L., Di Donna, A., 2013. Energy Geostructures: Innovation in Underground Engineering, Energy Geostructures: Innovation in Underground Engineering. https://doi.org/10.1002/9781118761809

Mayer, P.-M., Franzius, J.N., 2010. Thermische Berechnungen im Tunnelbau. Geotechnik 33, 145–151.

Moormann, C., Buhmann, P., Friedemann, W., Homuth, S., Pralle, N., 2016. Tunnel geothermics - International experience with renewable energy concepts in tunnelling / Tunnelgeothermie - Internationale Erfahrungen zu regenerativen Energiekonzepten im Tunnelbau. Geomech. Tunn. 9, 467–480.

Nicholson, D.P., Chen, Q., Pillai, A., Chendorain, M., 2013. Developments in thermal piles and thermal tunnel lining for city scale GSHP systems. Thirty-Eighth Work. Geotherm. Reserv. Eng.

Nicholson, D.P., Chen, Q., Silva, M. De, Winter, A., Winterling, R., 2014. The design of thermal tunnel energy segments for Crossrail , UK 167.

Ogunleye, O., Singh, R.M., Cecinato, F., Chan Choi, J., 2020. Effect of intermittent operation on the thermal efficiency of energy tunnels under varying tunnel air temperature. Renew. Energy 146, 2646–2658. https://doi.org/10.1016/j.renene.2019.08.088

Pahud, D., 2013. A case study: the Dock Midfield of zurich Airport, in: Laloui, L., Di Donna, A. (Eds.), Energy Geostructures: Innovation in Underground Engineering. ISTE Ltd and John Wiley & Sons Inc, pp. 281–295.

Preene, M., Powrie, W., 2009. Ground energy systems: from analysis to geotechnical design. Géotechnique 59, 261–271. https://doi.org/10.1680/geot.2009.59.3.261

Soga, K., Rui, Y., 2016. Energy geostructures, in: Rees, S.J. (Ed.), Advances in Ground-Source Heat Pump Systems. Woodhead Publishing, pp. 185–221. https://doi.org/https://doi.org/10.1016/B978-0-08-100311-4.00007-8

Zhang, G., Guo, Y., Zhou, Y., Ye, M., Chen, R., Zhang, H., Yang, J., Chen, J., Zhang, M., Lian, Y., Liu, C., 2016. Experimental study on the thermal performance of tunnel lining GHE under groundwater flow. Appl. Therm. Eng. 106, 784–795. https://doi.org/10.1016/j.applthermaleng.2016.06.041

548 Zhang, G., Xia, C., Yang, Y., Sun, M., Zou, Y., 2014. Experimental study on the thermal performance of tunnel lining ground heat exchangers.
549 Energy Build. 77, 149–157. https://doi.org/10.1016/j.enbuild.2014.03.043
550